1. Discrete Spectral Lines – DRAFT, INCOMPLETE

Discrete spectral features are useful for the following:

abundance of elements too low to contribute to the continuous opacity at any wavelength

sample wide range of atmospheric depths, in particular, cores of strongest lines formed much closer to surface than wings/continuum, so can probe upper atmosphere levels, reaching in some cases the chromosphere, just above the temperature minimum

precision radial velocities, including planet searches

much more sensitive to velocity fields on/near stellar surface due to much narrower frequency range

isolate orbital motions for individual stars in the spectrum of a binary star

2. Reminder Re Sources of Continuum Opacity

The main source of continuum opacity in cool stars is H−, which has only one bound state and an ionization potential of 0.75 eV. In hotter stars, the H bound-free and free-free opacities dominate. The appended figures indicating the contributions of the various sources as a function of temperature and frequency are taken from Gray, 3rd edition.
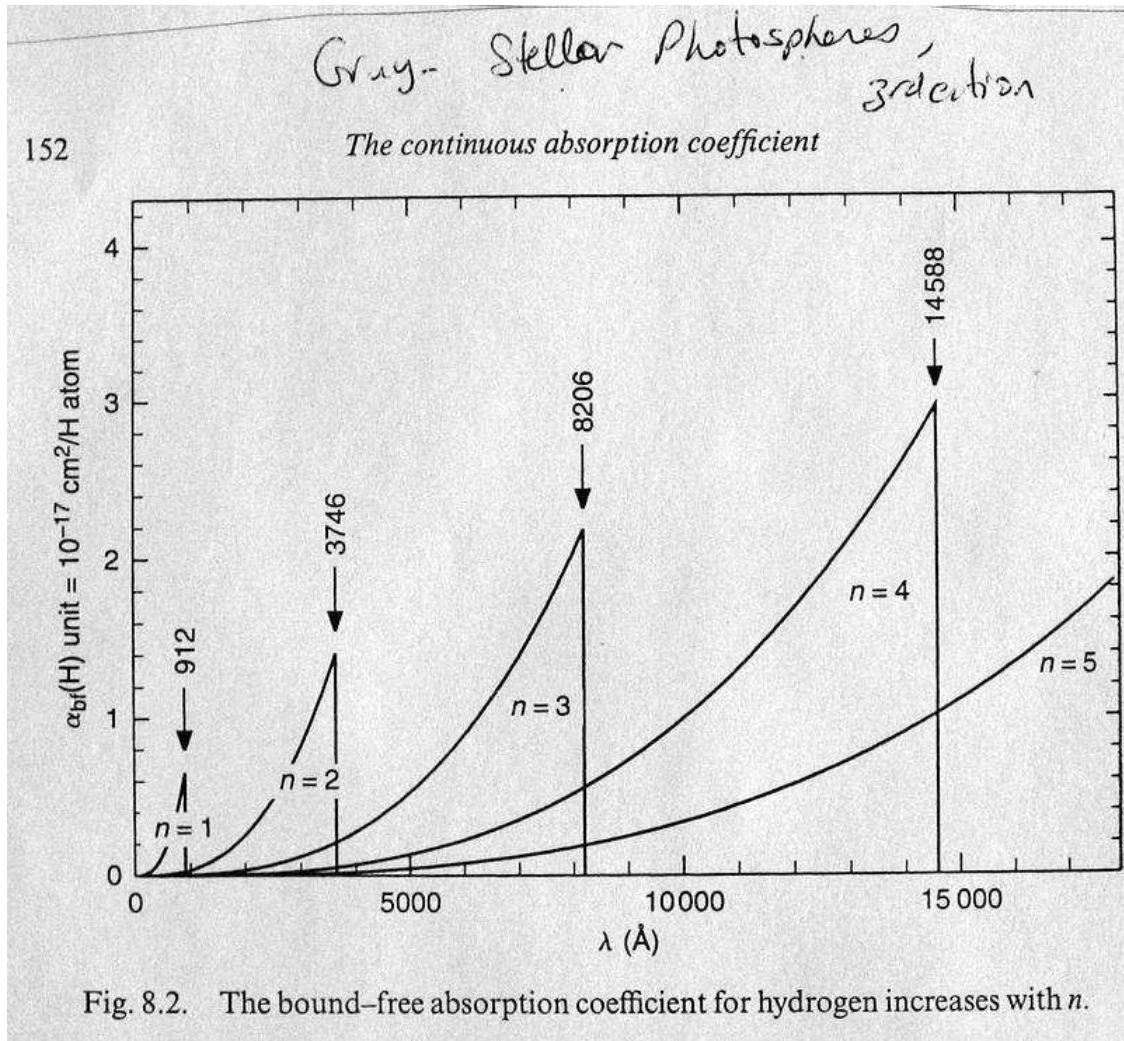
Gray – Stellar Photospheres,
3rd edition

The continuous absorption coefficient

Fig. 8.2. The bound–free absorption coefficient for hydrogen increases with n.

Fig. 1.— The bound-free absorption coefficient for H. (Fig. 8.2 of Gray)

The negative hydrogen ion (Gray 3rd ed)
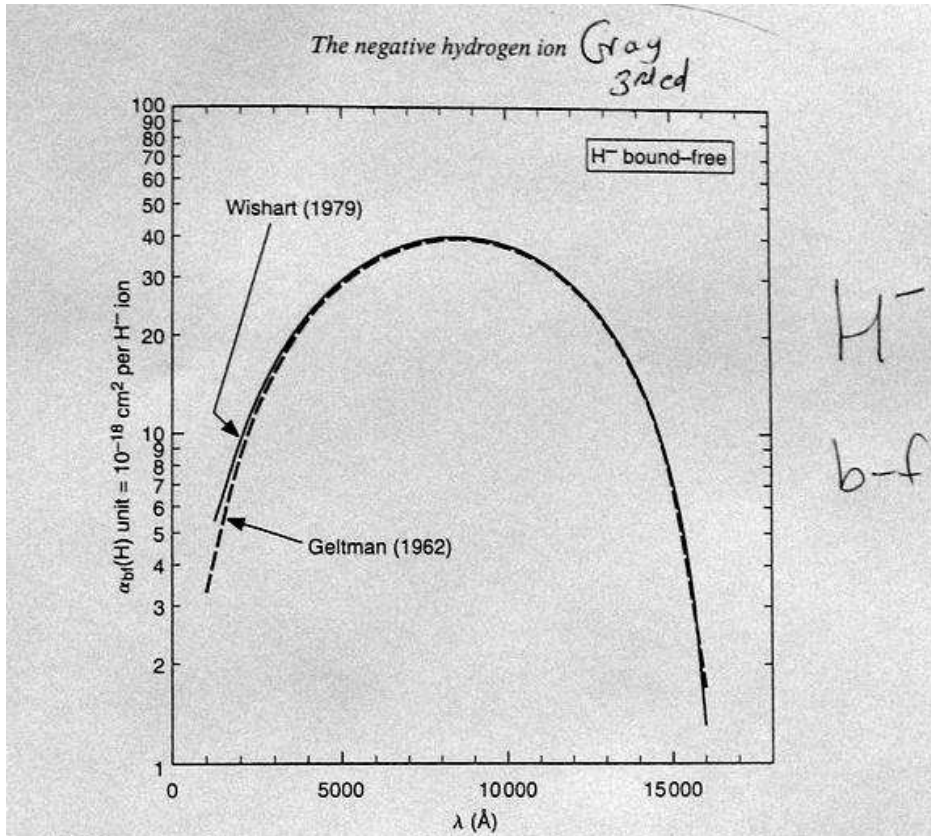
H⁻ bound–free

Wishart (1979)

Geltman (1962)

H⁻ b–f

Fig. 8.3. The absorption coefficient of the negative hydrogen ion shows a maximum near 8500 Å. Two calculations are compared.

Other hydrogen continuous absorbers

H⁻ free–free

2520 K

5040 K
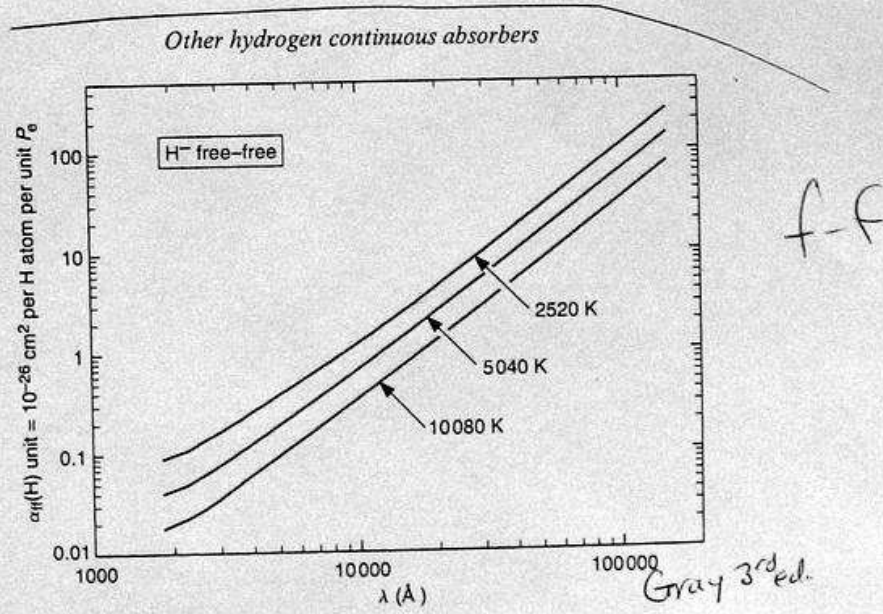
10080 K

f–f

Gray 3rd ed.

Fig. 8.4. The free-free absorption coefficient of the negative hydrogen ion increases rapidly with wavelength. The stimulated emission factor is included here.

Fig. 2.— The bound-free and free-free absorption coefficient for H^-. (Fig. 8.4 of Gray)

Gray – Stellar Photospheres
3rd edition

160   *The continuous absorption coefficient*

Fig. 8.5.   (a) Absorption coefficients per unit electron pressure are compared for a temperature of 5143 K. The absorption is dominated by the H^-_{bf} ion. The stimulated-emission factor has been included in these comparisons (all panels). (b) The absorption coefficients per unit electron pressure are compared for a temperature of 6429 K. The absorption is dominated by the two components of the H^- ion. (c) The absorption coefficients per unit electron pressure are compared for a temperature of 7715 K. Here absorption from the H^- ion is dropping back compared to the cooler cases, while neutral hydrogen has grown with increasing temperature. (d) The absorption coefficients per unit electron pressure are compared for a temperature of 11 572 K. The absorption is now dominated by the neutral hydrogen component. Notice the large increase in the absolute scale of the ordinate compared to the previous panels.
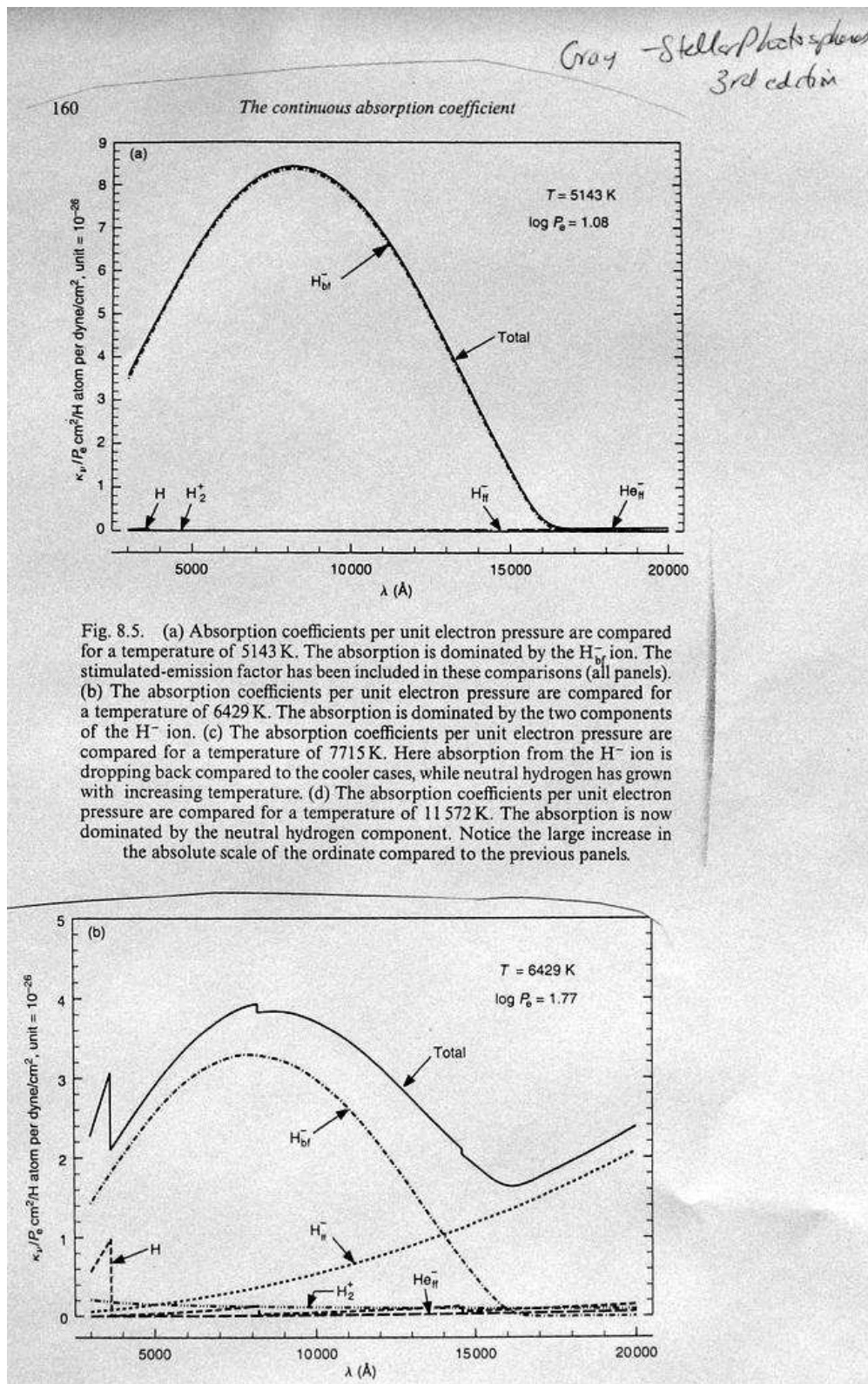
Fig. 3.— The contributions to the total opacity for low temperatures. (Fig. 8.5 of Gray)
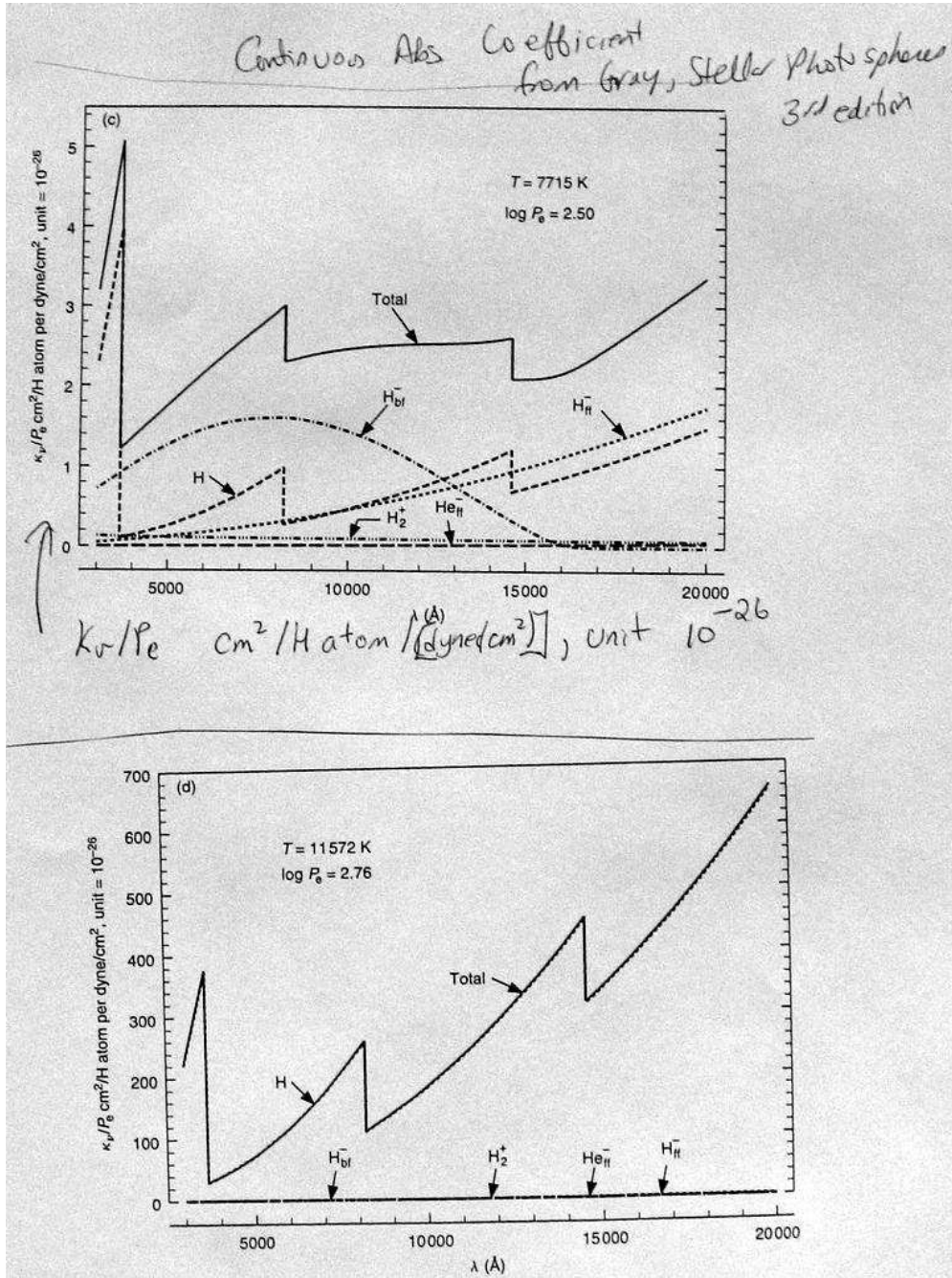
Fig. 4.— The contributions to the total opacity for higher temperatures where the contribution from H dominates. (Fig. 8.5 of Gray, additional panels)

3.   The Line Absorption Coefficient

We assume a solution for the model atmosphere with the desired values of the stellar parameters T_{eff} and $\log(g)$ (and chemical composition, X, Y, Z) has been created using the appropriate continuous opacity. We assume that individual lines are then added, but they do not modify the $T(\tau_c)$ structure established using the equations of stellar structure appropriate for the atmosphere with the continuous opacity sources.

The specification of a specific spectral line includes the element X of abundance $A(X)$ and stage of ionization N (N = nuetral or singly ionized or ...) which give rise to the line. The excitation potential χ for the lower state of the transition is also required as is specification of the central frequency $\nu_0 = \Delta(E_{ul})/h$ where E_{ul} is the energy difference between the upper and lower electronic configurations/states of this transition.

The profile of this line is a normalized function of ν which we call $\phi(\nu)$ peaked at ν_0.

$$\int_0^\infty \phi(\nu)d\nu \;=\; 1.$$

To find the profile function, we need to find $x(t)$ for the radiating electron/particle, then Fourier transform that to get $f(\omega)$, where $\omega = 2\pi\nu$.

If several different types of broadening with different functional forms for $f(\omega)$ contribute, we need to convolve those to obtain the final profile function. Convolution in physical space is equivalent to multiplication in Fourier space, so it may be easier to calculate this in Fourier space.

The damped harmonic oscillator,

$$\frac{d^2x}{dt^2} \;=\; -\,\omega_0^2\,x - \gamma\frac{dx}{dt}$$

has the solution

$$x(t) = x_0 e^{i\omega_0 t} e^{-\gamma t/2}$$

The Fourier transform of this solution $x(t)$ is the Lorenz function,

$$\phi(\omega) \propto \frac{\Gamma}{(\nu - \nu_0)^2 + \Gamma^2}$$

where $\Gamma = \gamma/(4\pi)$.

Natural damping (from considering the energy lost by a radiating electron) is always present, and is effectively a damped harmonic oscillator. Hence in frequency space it appears as a Lorenz profile. For natural damping,

$$\gamma = \frac{2e^2\omega^2}{3mc^3}$$

Natural damping has a FWHM which is constant in wavelength, $\Delta\lambda_{1/2} = 1.2 \times 10^{-4}$ Å. This values is both fixed and small compared to other sources of line broadening.

Various collision perturbation terms also lead to a Lorenz profile, or something quite close to that function.

Note that the convolution of two Lorenz profiles is also a Lorenz profile with $\Gamma_{total} = \Gamma_1 + \Gamma_2$.

Doppler broadening, from thermal motions, reflects the Maxwellian velocity distribution, and has a Gaussian profile function. The Fourier transform of a Gaussian is a Gaussian.

$$\phi(\nu) \;\propto\; e^{-\frac{v^2}{\beta^2}}\,\frac{dv}{\beta} \;\propto\; e^{-\frac{\Delta\nu^2}{\Delta\nu_D^2}}$$

where $\beta^2 = 2kT/m$ (β is the mean thermal speed) and $\Delta\nu_D \;=\; \nu_0\beta/c$.

The Voigt profile, which does not have a simple analytical form, is the convolution of a damping profile and thermal broadening.

4.   Forming the Line Absorption Coefficient

Given the normalized profile function $\phi(\nu)$, the cross section/radiating atom is

$$\sigma(\nu) \;=\; \frac{\pi e^2}{mc}f\phi(\nu)$$

The first factor is a cross section, πr_e^2, multiplied by the quantum mechanical correction factor f (ranging from about 2 to 10^{-4} depending on whether the transition is permitted by the selection laws of QM or not.

To get $\alpha(\nu)$, the absorption coefficient/cm of the line of element X in the correct ionization state and correct lower level, we set:

$$\alpha(\nu) \;=\; \frac{\pi e^2}{mc}(gf)\,n(X)\,[IF(X)]\,e^{-\chi/kT}\,\phi(\nu)$$

The latter terms give the number of atoms of type X in the correct ionization stage and electronic level, which contains the ionization fraction $IF(X)$ (the fraction of atoms of element X in the desired ionization stage), the excitation potential χ, and statistical weight of the lower level g. The last term is the normalized line profile function.

At large $\Delta\nu$, far from the line center, $\alpha(\nu) \propto 1/\Delta\nu^2$, while close to the line center, the

Doppler core dominates.

5. Collisional Broadening

Two treatments, one collision at a time (impact approximation) or statistical. First has a Lorentz profile where $\gamma = 2/\tau$, τ is the mean time between collisions.

For an impact parameter ρ and a perturber number density n_p we have $1/\tau = \pi\rho^2 n_p v_{rel}$, where the relative velocity of the radiating atom and the perturber is used. A smaller impact parameter means a collision which produces a larger perturbation. Such close collisions, for a given number density of perturbers, are rare. The impact approximation will be valid when the duration of a collision, approximated by ρ/v_{rel}, is less than τ, where τ is the mean time between collisions.

We assume an interaction $\delta\omega = C_p/r^p$, where C_p is a constant. $p = 2$ for the linear Stark effect (H + charged particle), $p = 6$ for Van der Waals broadening (atom A + atom B, both neutral).

The total phase shift for the collision is

$$\eta(t) \;=\; \int_{-\infty}^{t} \Delta\omega(s)ds \qquad \eta(\infty) \;=\; \int_{-\infty}^{\infty} \Delta\omega(t)dt \;=\; \int_{-\infty}^{\infty} \frac{C_p}{[(vt)^2 + \rho^2]^{p/2}}dt$$

If $\eta(\infty) > \eta_0$, colisions are effective at broadening the line. Choose $\eta_0 = 1$ to get the Weiskopf radius, i.e. the maximum impact parameter of interest for the impact approximation to be valid, ρ_0.

In the statistical theory, consider only the nearest neighbor, at distance d. We need the probability distribution for d, $P(d)$, then take $P(d)C_p/d^p$. This results in a function which is almost a Lorentz profile.

In practice one can adopt the following approximation for Van der Waals broadening $(p = 6)$ (hydrogen broadening with $p = 2$ requires a more careful treatment)

$$\Gamma(p = 6) \;=\; 17C^{2/5}v^{3/5}n_p \text{ Hz}, \qquad C \;=\; 6.5 \times 10^{34}\, \frac{R_K^2}{a_0^2}$$

where a_0 is the Bohr radius for hydrogen and R_K is the radius in the radiating atom of the relevant electronic state in units of the Bohr radius.

Since $\gamma \propto n_p$, the number density of the perturbers, for a fixed temperature, it increases as the pressure increases. Hence γ increases with surface gravity for a fixed T_{eff} stellar model atmosphere.

6.   Radiative Transfer Issues

The addition of absorption under the assumptions outlined in the introductory paragraphs basically means a shifting of the optical depth – physical depth relation previously established using only the continuous opacity sources. Adding in the line opacity, we determine the value of $\tau(line)$, which includes both the line and continuous opacities, for a given physical depth. This will give a lower surface emitted flux than when just the continuous opacity is included for a model atmosphere where temperature increases inward.

Note that $\tau(line) = \tau(cont)$ for frequencies far from the line center, where $\alpha(\nu)$ is very small and can be ignored. At frequencies near the line center, for any physical depth z, $\tau(line) > \tau_C$.

7. Approximations for Equivalent Width

We define $A(\nu)$ as the fraction of the continuum absorbed using the computed detailed line profile as a function of frequency,

$$A(\nu) \;=\; \frac{F_C - F_{line}(\nu)}{F_C}.$$

when we take into account the presence of the line by using $\kappa = \kappa(cont) + \kappa(line)$. We evaluate F_C near ν_0, the frequency of the line center.

We define the residual intensity $R(\nu)$ as $R(\nu) = F_{line}(\nu)/F_C$. The equivalent width

$$W_\nu \;=\; \int_0^\infty A(\nu)d\nu.$$

W_λ is often used as well. W_ν represents the frequency width of the line if viewed as an inverted top hat, with 100% absorption of the continuum over that frequency interval. Ditto for W_λ with regard to a wavelength interval.

To get approximate solutions, we assume that $F(\tau = 0, \nu)$ is $B_\nu(T : \tau = 2/3)$. We then derive for weak lines, i.e. those with $\kappa_{line} << \kappa_C$ at the line center,

$$A(\nu) \;=\; \frac{2}{3}\frac{\kappa_{line}(\nu)}{\kappa_C}\frac{dlnB_\nu}{d\tau_C}, \quad \text{evaluated at } \tau_C = 2/3.$$

Thus for weak lines,
$$W \propto \frac{n(X)\ IF(X)\ e^{-\chi/kT}gf}{\Delta\nu_D\ \kappa_C}.$$

For strong lines, where the damping wings dominate,

$$W \;\propto\; \sqrt{\Gamma\ n(X)\ (IF)\ e^{-\chi/kT}gf/\kappa_C}.$$

In lines of intermediate strength, the line center absorbtion is strong enough that the flux is the minimum flux level, corresponding to $B_\nu(T : \tau = 0)$, which is about 20% of the continuuum flux. Recall that the continuum flux can be approximated as originating at $\tau_c = 2/3$; see the notes on radiative transfer. The whole Doppler core gradually is brought down to this minimum flux level for lines of intermediate strength. In this case, $W \propto log[n(X)IFe^{-\chi/kT}gf/(\Delta\nu_D\kappa_C)]$. Eventually the whole Doppler core has $F(\nu)$ at this minimum. At that point the wings begin to become important, and we switch to the strong line case.

Fig. 9.10. Sharp differences in opacity can greatly shift the depth of formation, as illustrated here for a model where the Balmer discontinuity of κ_ν is large.

S_0 = ratio to Solar $T(\tau)$

for scaled Solar models

$$T(\tau) = \frac{T_{eff}}{T_{eff}(\odot)} T_0(\tau) \quad [\text{grey case}]$$

$$= S_0 \, T_0(\tau) \quad (\text{non-grey, general})$$

from Gray, Stellar Photospheres, 3rd ed.
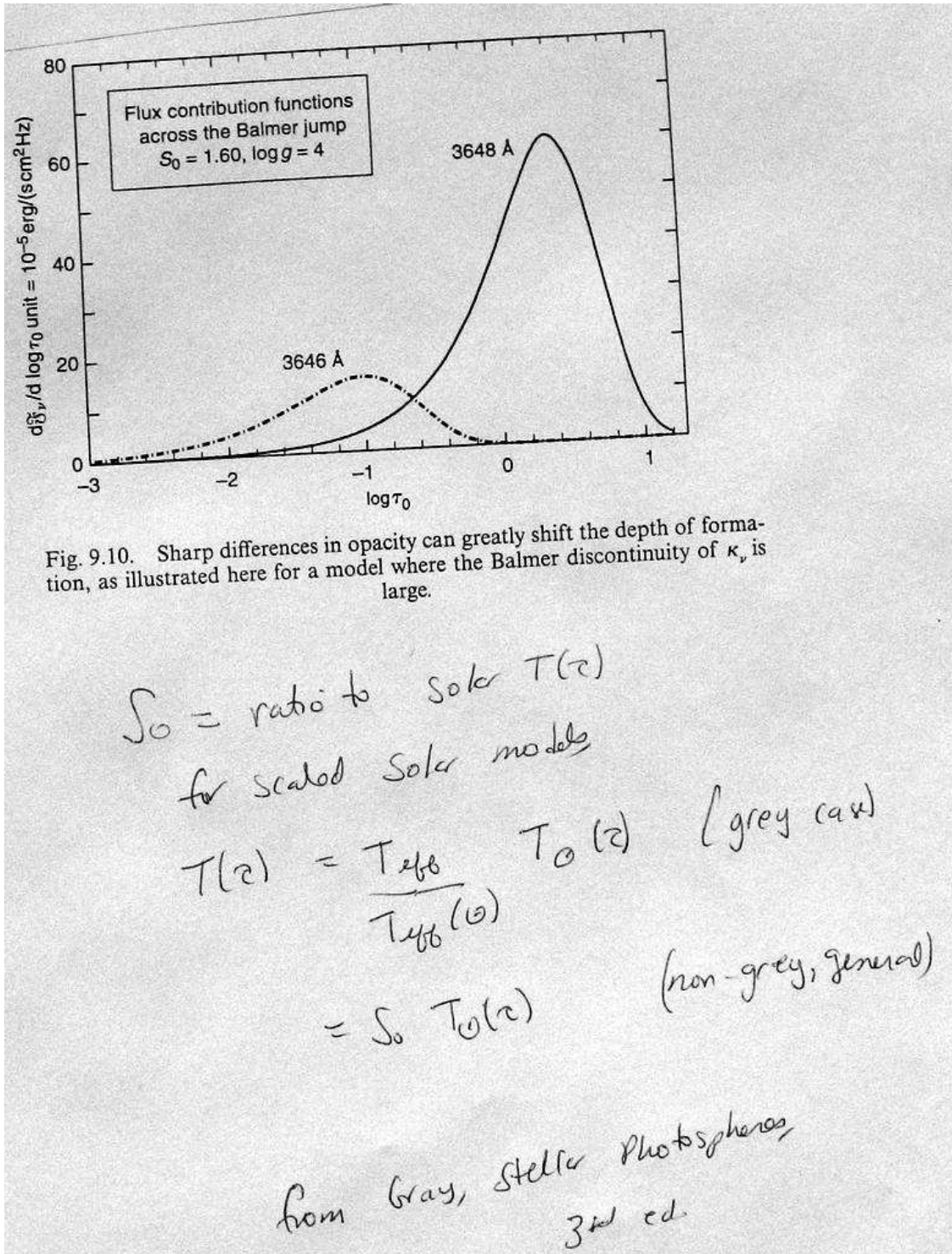
Fig. 5.— The contribution to the flux on the blue and red side of the Balmer jump as a function of depth in the atmosphere. The much higher opacity on the blue side of the Balmer jump means that the flux is coming from shallower, cooler layers. This is Fig. 9.10 of Gray.
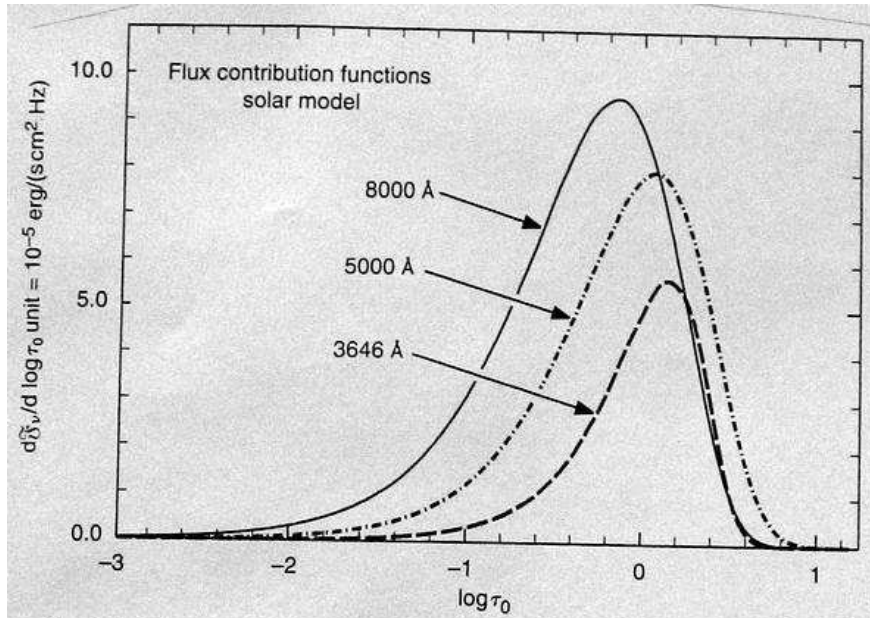
Fig. 9.9. Flux contribution functions show the relevant depths when computing the flux integral and they indicate the depths of formation, i.e., the layers from which the flux comes.
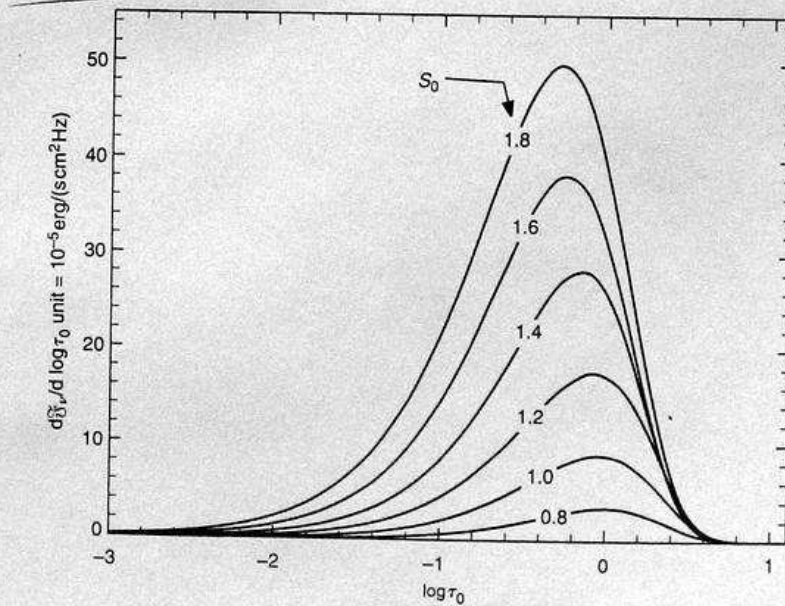
Fig. 9.11. Contribution functions at 6000 Å are shown for a run of models having different effective temperatures (S_0). The hotter models obviously produce more flux (area) and show a slight decrease in the depth of formation.

Fig. 6.— The contribution to the emitted flux in the continuum at various wavelengths as a function of depth in the atmosphere. S_0 is T_{eff}/T_{eff}(Sun). This is Fig. 9.9 of Gray.

Table 11.1. *Types of pressure broadening.*

Type	Lines affected	Perturber
Linear Stark	Hydrogen	Protons, electrons
Quadratic Stark	Most lines, especially in hot stars	Ions, electrons
van der Waals	Most lines, especially in cool stars	Neutral hydrogen

α

2
4
6

$\Delta W \propto 1/R^n$
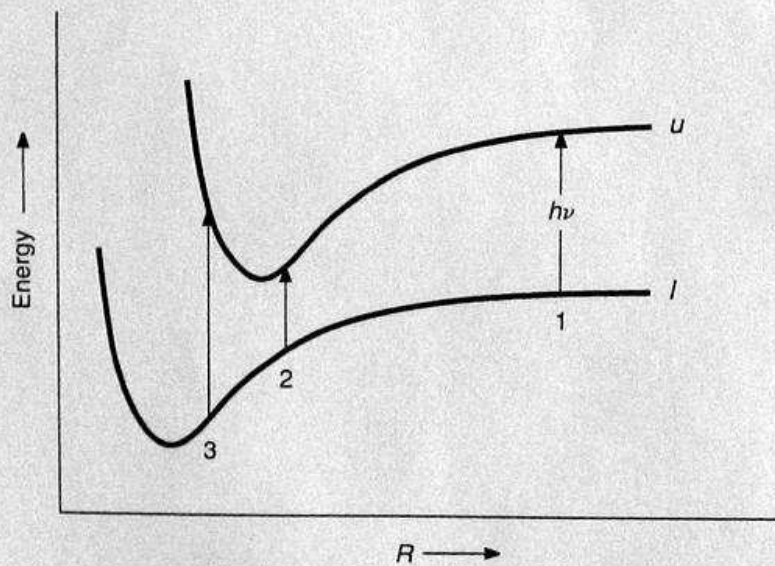
Fig. 11.2.   The energies associated with the upper and lower atomic levels on a transition depend on the distance R to the perturber. The transition energy can be either less (2) or greater (3) than the unperturbed value (1).

Fig. 7.— The perturbation of the upper and lower levels of an atomic transition. The upper level has electrons at larger distances from the atomic nucleus in the mean, hence is more easily perturbed by collisions. This is Fig. 11.2 of Gray.

from Gray, Steller Photospheres 3rd ed.
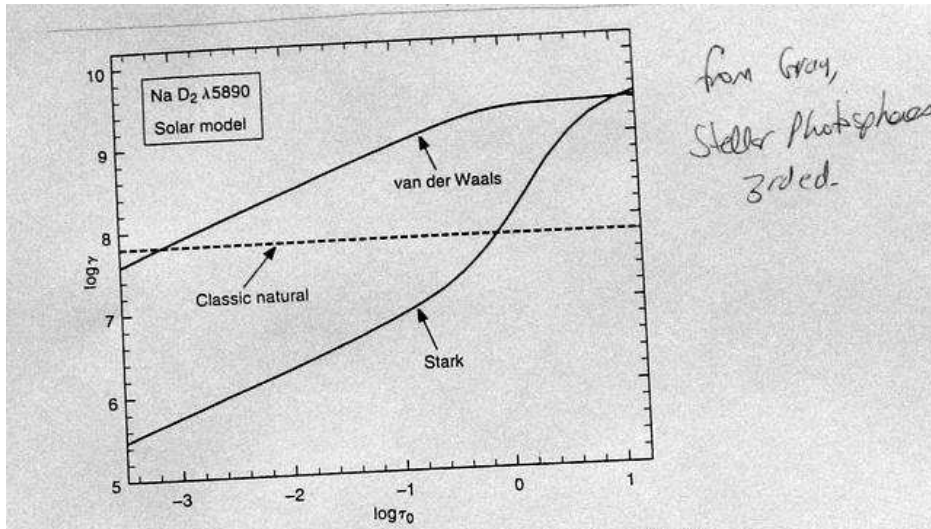
Fig. 11.4. Damping constants for the Na I D$_2$ line are shown as a functi of depth in a solar model. The van der Waals damping constant is comput using Eq. (11.9). The Stark damping constant comes from Eq. (11.27). F omparison, the natural radiation damping according to Eq. (11.13) is show

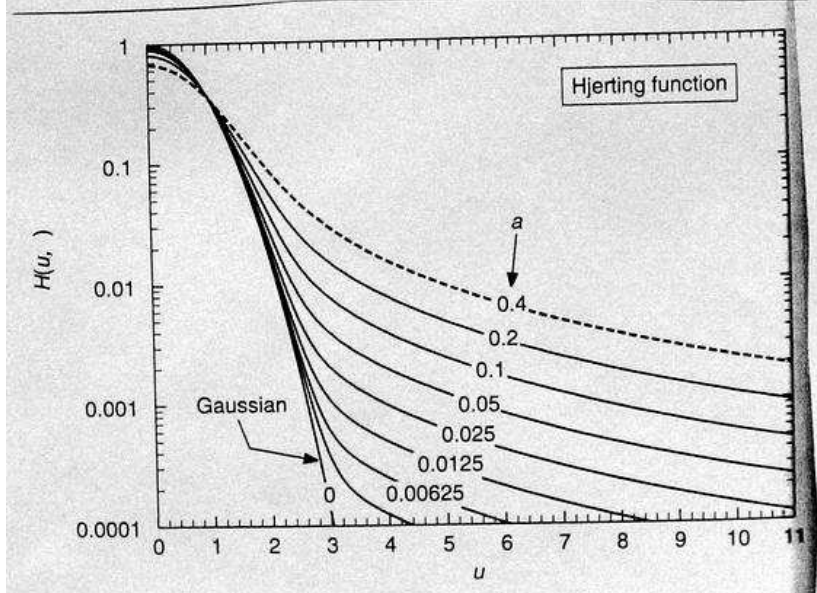$$C_6 = 0.3 \times 10^{-30} \left[\frac{1}{(I - \chi - \chi_\lambda)^2} - \frac{1}{(I - \chi)^2} \right],$$

Fig. 11.10. Hjerting functions are plotted with a logarithmic ordinate to emphasize the growth of the wings with increasing damping parameter a.

Voigt profile $V(a, u) = \dfrac{H(a u)}{\sqrt{\pi}\, \Delta \nu_D}$

Fig. 8.— Upper panel: damping constants for the NaI D line as a function of depth in the solar atmosphere calculated in several diferent ways. Lower panel: The Hjerting (Voigt) function which describes the line profile, with both Gaussian and damping contributions. This is Fig. 11.4 (top) and 11.10 (bottom) of Gray.
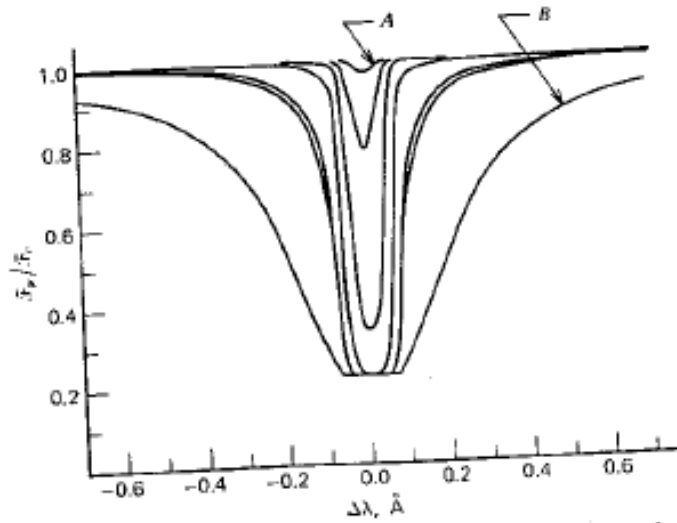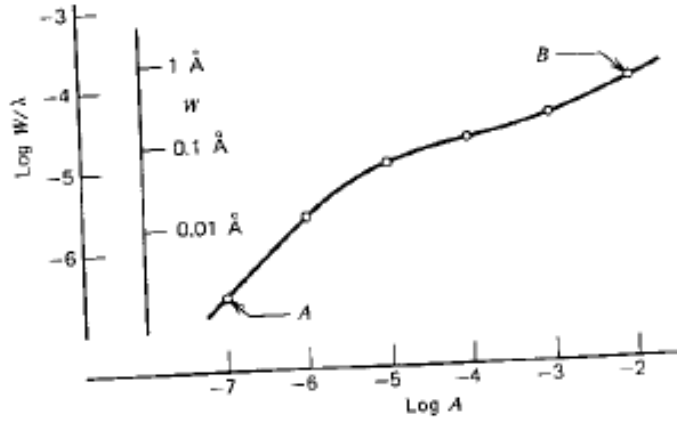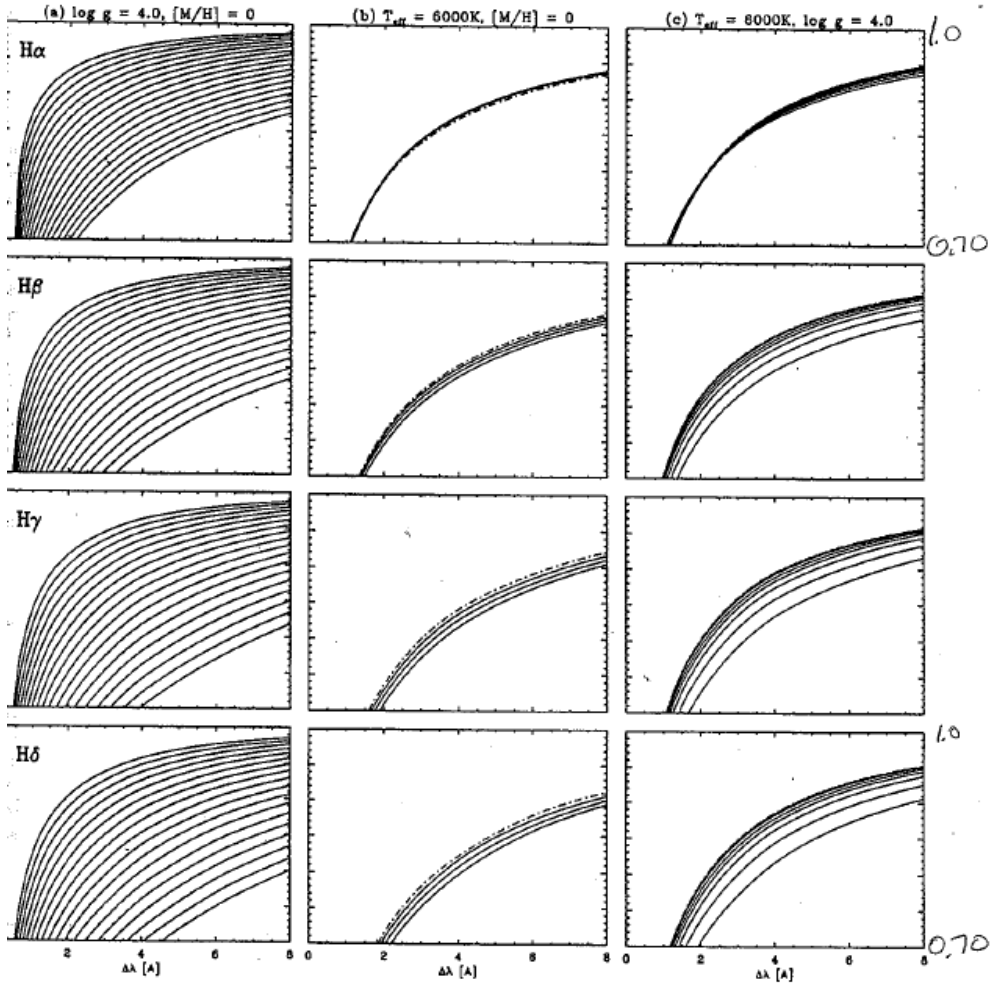
Fig. 13-12 The line strength dependence on chemical abundance of the absorbing species is shown. At the bottom the increasing profile strength is illustrated for decade steps in abundance. At the top is the curve of growth for this same line. The dots on the curve of growth correspond to the profiles below. (Computations based on a model with $S_0 = 0.87$ and $g = 10^4$.)

Fig. 9.— Upper panel: curve of growth, lower panel: a series of line profiles as abundance changes by a factor of 10. Note the presence of the Doppler core and the damping wings (for the higher abundances) in the line profiles. This is Fig. 13.12 of Gray.

Fuhrman, Axer + Gehren, 1993, A+A, 271, 451
Balmer Lines In Cool Dwarf Stars

I. Variation of Balmer line profiles with stellar parameters. (a) *effective temperatures*, ranging from 5000 K (top) to 6700 K (bottom) with crement of 100 K. (b) log *surface gravity*, in steps of $\Delta \log g = 0.5$ from 3.0 to 4.5 (dot-dashed profile). (c) *metal abundances*, [M/H] g from −3.5 (top) to 0.0 (bottom) with steps of 0.5. All calculations assume $\alpha = y = 0.5$

Fig. 10.— Theoretical Balmer line profiles from Fuhrman, Axer & Gehren, 1993, A&A, 271, 451. Left panels - F_{eff} chaging from 5000 K to 6700 K (steps 100 K), middle panels - changing $\log(g)$, right panels - changing metallicity. Vertical axis is residual intensity from 0.70 to 1.0 in each panel.
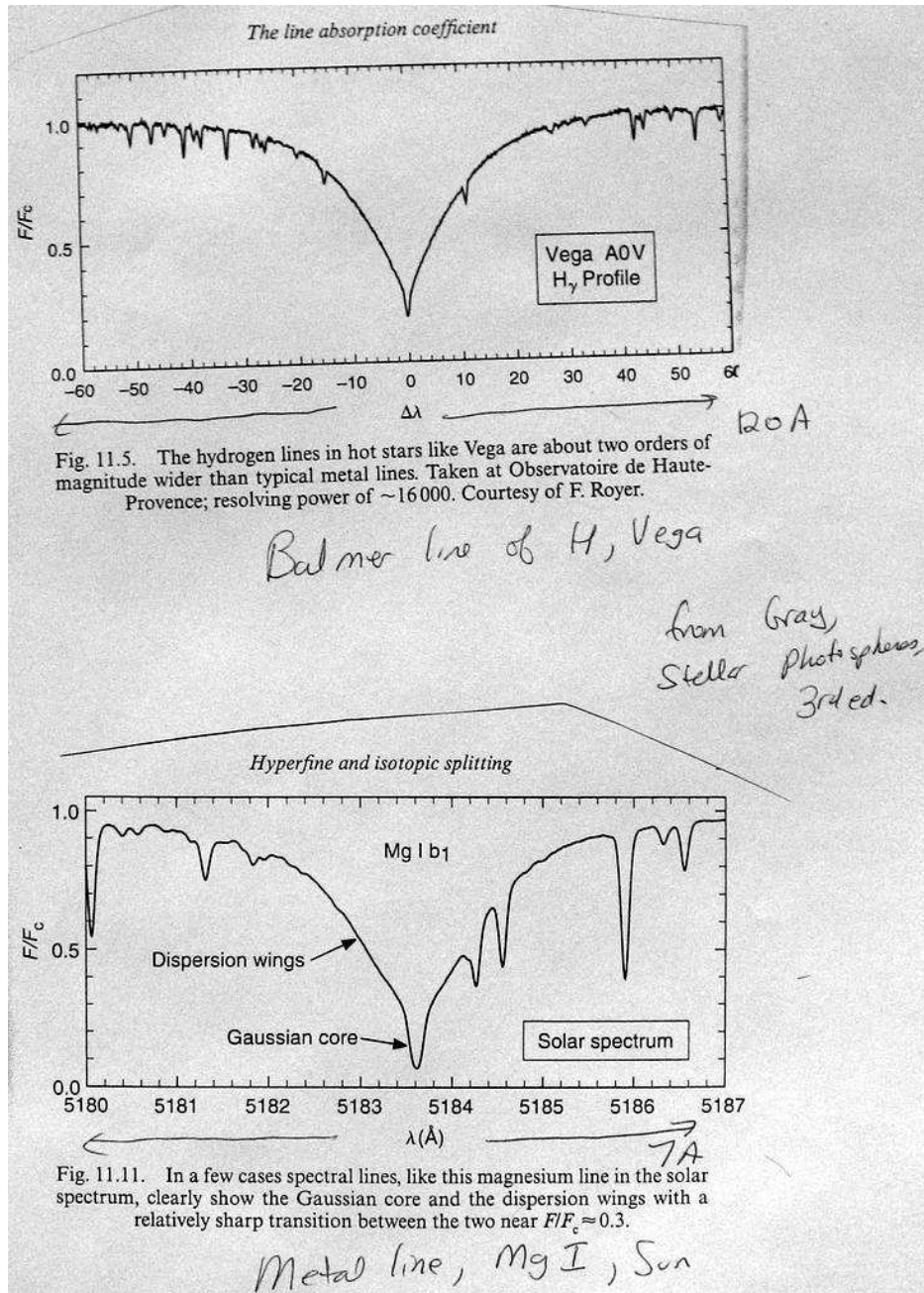
The line absorption coefficient

Vega A0V
H$_\gamma$ Profile

Fig. 11.5. The hydrogen lines in hot stars like Vega are about two orders of magnitude wider than typical metal lines. Taken at Observatoire de Haute-Provence; resolving power of ~16 000. Courtesy of F. Royer.

Balmer line of H, Vega

120 A

from Gray, Stellar Photospheres, 3rd ed.

Hyperfine and isotopic splitting

Mg I b$_1$

Dispersion wings

Gaussian core

Solar spectrum

Fig. 11.11. In a few cases spectral lines, like this magnesium line in the solar spectrum, clearly show the Gaussian core and the dispersion wings with a relatively sharp transition between the two near $F/F_c \approx 0.3$.

7 A

Metal line, Mg I, Sun

Fig. 11.— Upper panel: Strong Balmer lines in Vega. Lower panel: Strong MgI line in the solar spectrum. Note the presence of the Doppler core and the damping wings in the line profile. This is Fig. 11.11 of Gray.

Fuhrmann, Axer + Gehren, 1993, A&A, 271, 451

Balmer Lines in
Cool Dwarf Stars

K. Fuhrmann et al.: Balmer lines in cool dwarf stars. I   459
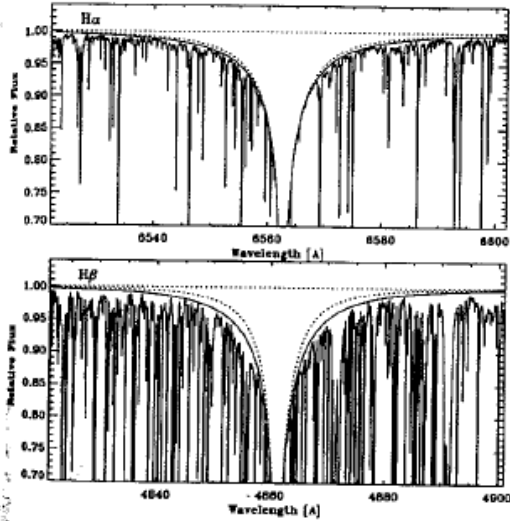
Fig. 8. Comparison of solar Balmer lines with profiles synthesized from a standard *ODF* solar model atmosphere with $\alpha = 0.5$ (continuous curve) and 1.5 (dotted curve)
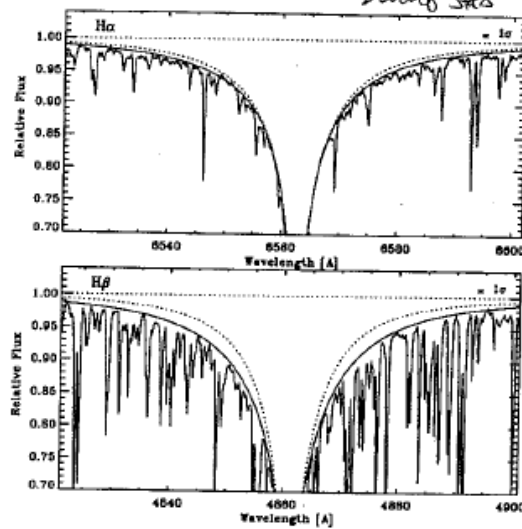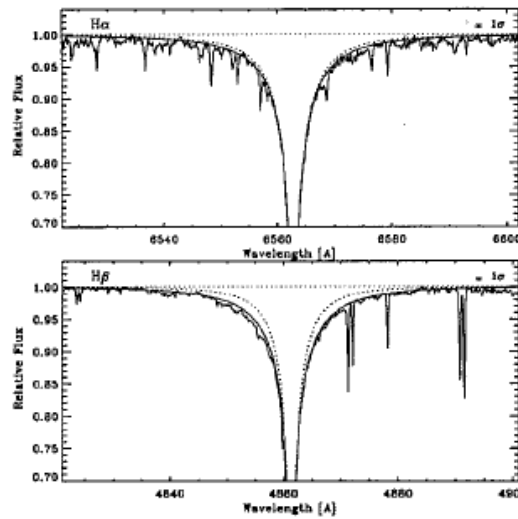
Sun

Fig. 9. Observed Balmer lines of Hα and Hβ in the spectrum of Procyon compared with synthesized profiles from a model atmosphere with $T_{eff} = 6500$ K, log $g = 4.0$ and [M/H] = 0 with $\alpha = 0.5$ (continuous) and 1.5 (dots)

Procyon

metal poor
cool dwarf

Fig. 10. Profile fits for Balmer lines in the spectrum of HD 140283. Stellar parameters are given in the text. Fit profiles again refer to $\alpha = 0.5$ and 1.5, respectively

Fig. 12.— Comparison of observed and theoretical Balmer line profiles (from Fuhrman, Axer & Gehren, 1993, A&A, 271, 451) for the Sun, Procyon, and a metal poor cool dwarf.
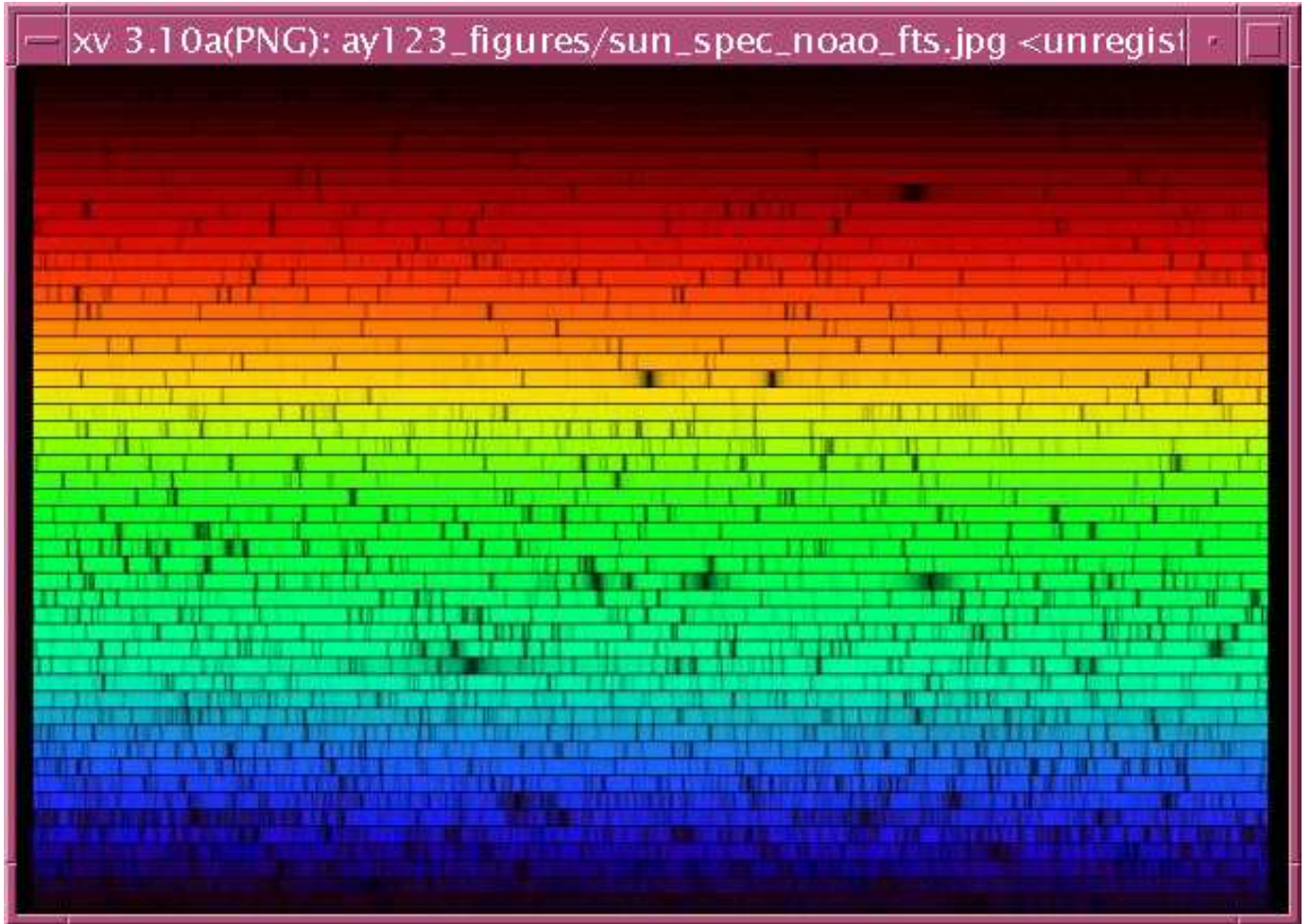
Fig. 13.— The Solar spectrum, NSO/FTS. Full spectral coverage over wavelength regime about 350 to 950 nm.
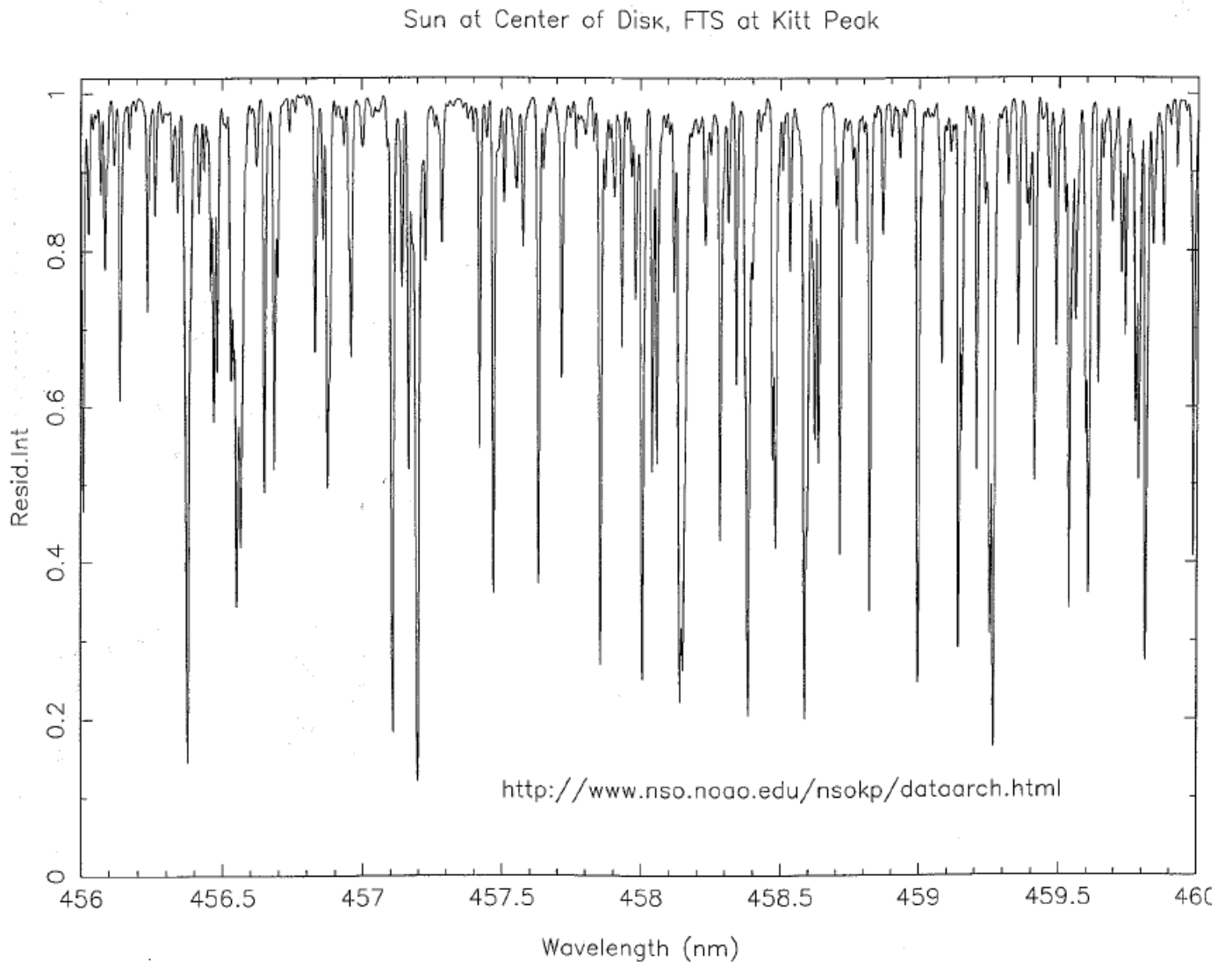
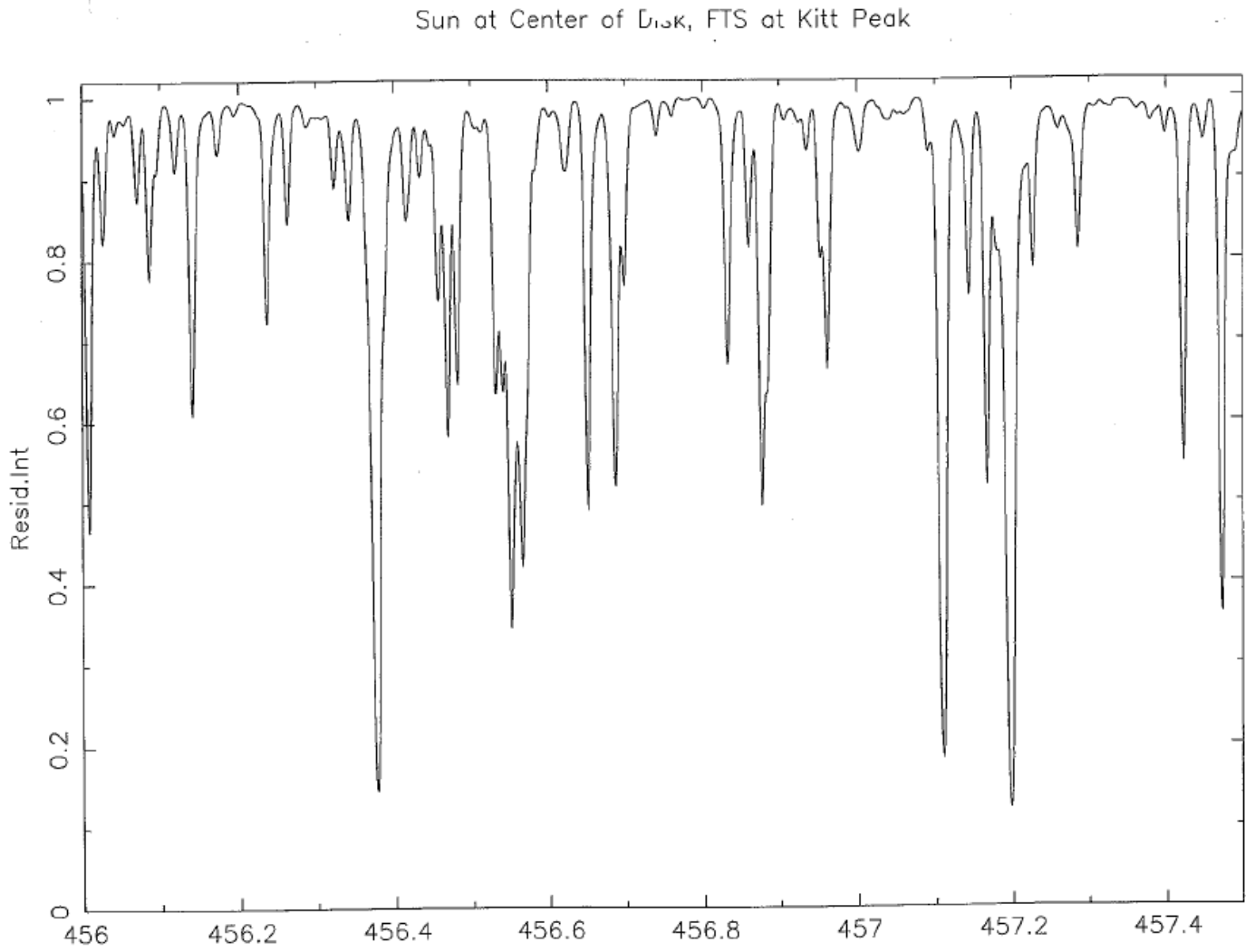Fig. 14.— A small piece of the Solar spectrum, NSO/FTS.

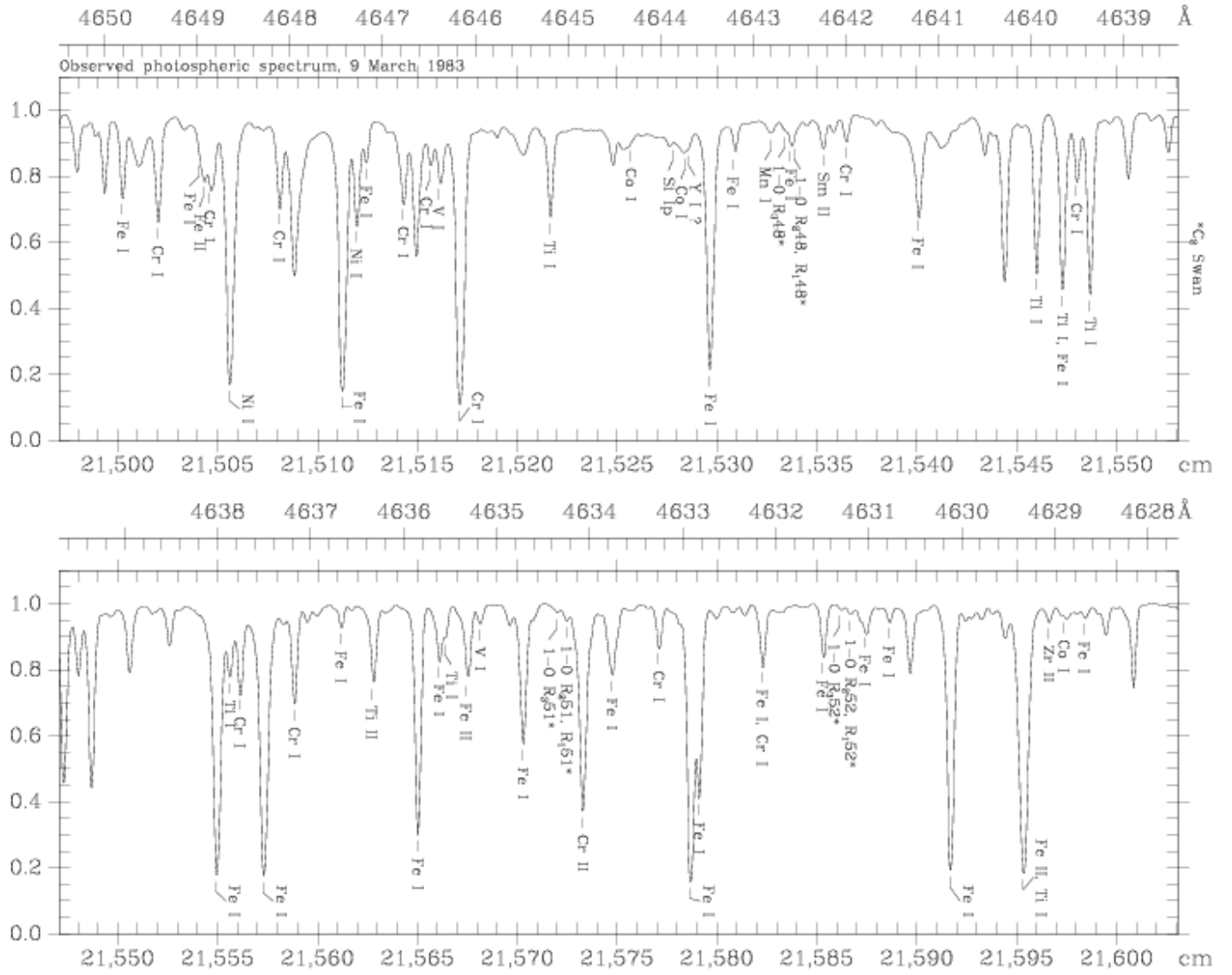Fig. 15.— A small piece of the Solar spectrum, NSO/FTS.

Fig. 16.— A small piece of the Solar spectrum, NSO/FTS, with the spectral lines identified.
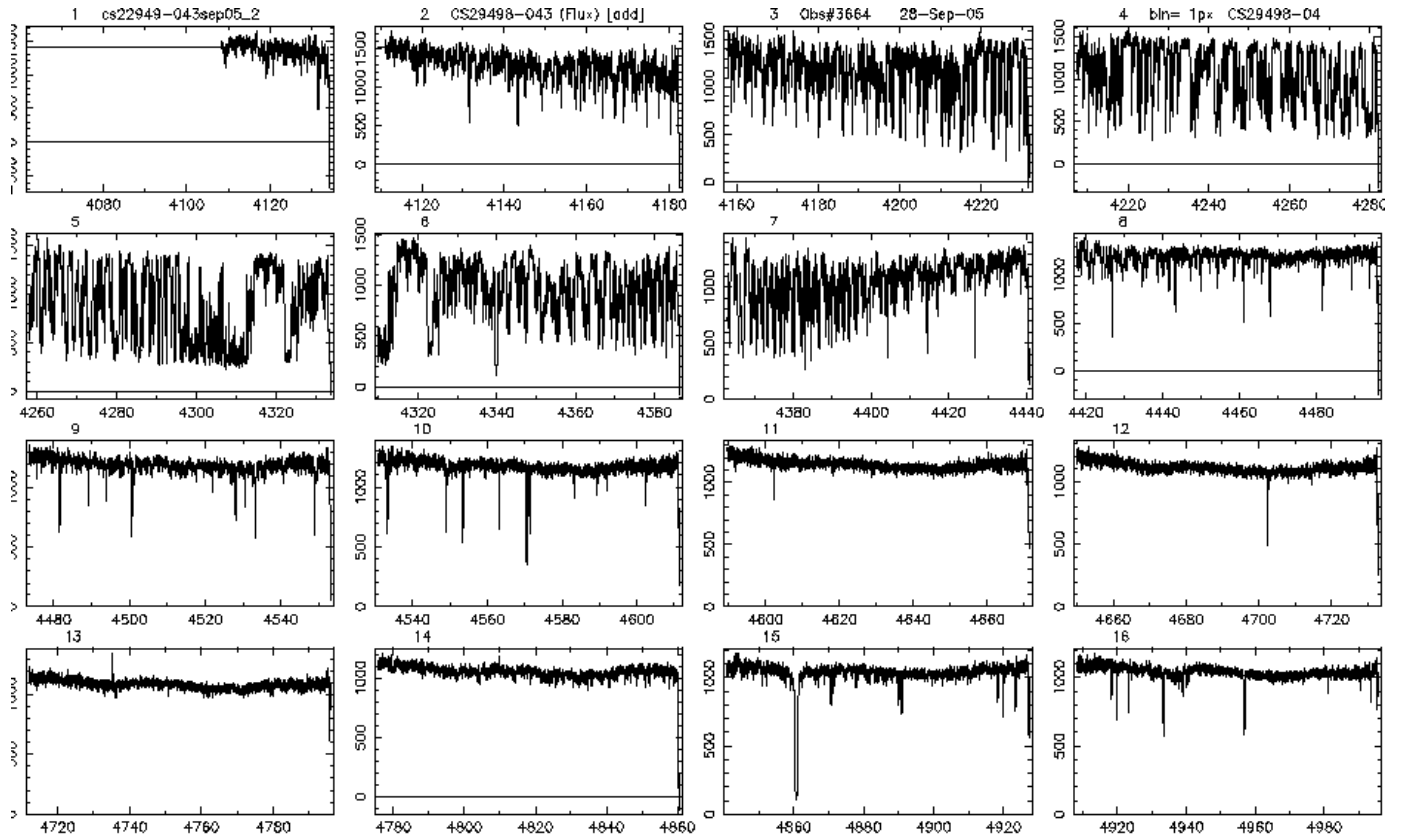
Fig. 17.— Part of a Keck/HIRES spectrum of an extremely metal-poor star with very strong CH bands. This is about 1/3 of the total spectral coverage one can obtain in a single exposure.

8. The Inglis – Teller Relationship

This relationship is used to predict the number density N by counting the lines in a series (often the Balmer series is used) that can be resolved as separate features up to the series limit. Because of the finite width of the lines, the lines can only be counted as separate up to a definite quantum number n_{max}, and this limiting value can be used to obtain the number density.

H lines are broadened by the linear Stark effect, as the perturbation is proportional to the electric field. Let r_0 be the mean interparticle distance. The perturbing atoms in this case are protons and electrons.

$$r_0 = [\frac{3}{4\pi N}]^{1/3}$$

Then $\Delta\omega_0 = C_p/r^p$, $C_p = 3$, $p = 2$.

The electric field $E = e/r_0^2 = e(4\pi N/3)^{2/3}$.

The change in energy of an electron in a H atom in the nth level due to this perturbing force is (recall that the radius of the electron in the nth level is $n^2 a_0$):

$$\Delta E_n = r_e e F = n^2 a_0 e^2 (4\pi N/3)^{2/3}.$$

The line series has transitions from lower state 2 (for the Balmer series) to upper level n, where the energy of level n is $13.6/n^2$ eV or $-e^2/(2n^2 a_0)$. We now look at separation of two adjacent lines, to levels n and to $n+1$. This is

$$\Delta E(n) = E_n - E_{n+1} = \frac{e^2}{2n^2 a_0} - \frac{e^2}{2(n+1)^2 a_0} \approx \frac{e^2}{2n^2 a_0}[1 - (1 - 2/n)] \approx \frac{e^2}{n^3 a_0}$$

The lines in the series merge and become undistinguishable when

$$\Delta E(n)/2 \;=\; \Delta E(perturb)$$

$$n^2 a_0 \; e^2 \; (4\pi N/3)^{2/3} \;=\; \frac{e^2}{2n^3 a_0}$$

The solution for the number density N of the perturbers is:

$$N \;=\; \frac{1}{n^{7.5}} \, [\frac{1}{2a_0^2(4\pi/3)^{2/3}}]^{1/5}.$$

Evaluating the constants gives, for N/cm^3,

$$log(N) \;=\; -\,7.5 \; log(n_{max}) + 23.48.$$

A better derivation, including a better theory of line broadening, gives

$$log(N) \;=\; -\,7.5 \; log(n_{max}) + 22.96.$$

A dwarf main sequence star might have $N \sim 10^{16}/\text{cm}^3$, which would predict $n_{max} = 9$. A supergiant might have a number density as low as $N \sim 10^{13}/\text{cm}^3$ in its atmosphere, which would lead to $n_{max} = 23$. This difference is easily discernable from inspection of the spectra of the two stars, even at moderate resolution.

Thus one can deduce the gravity of a star from the Inglis–Teller relationship. Ionization balance between abundances deduced from spectral lines of the neutral and of the ionized species of the same element can also be used for this purpose.
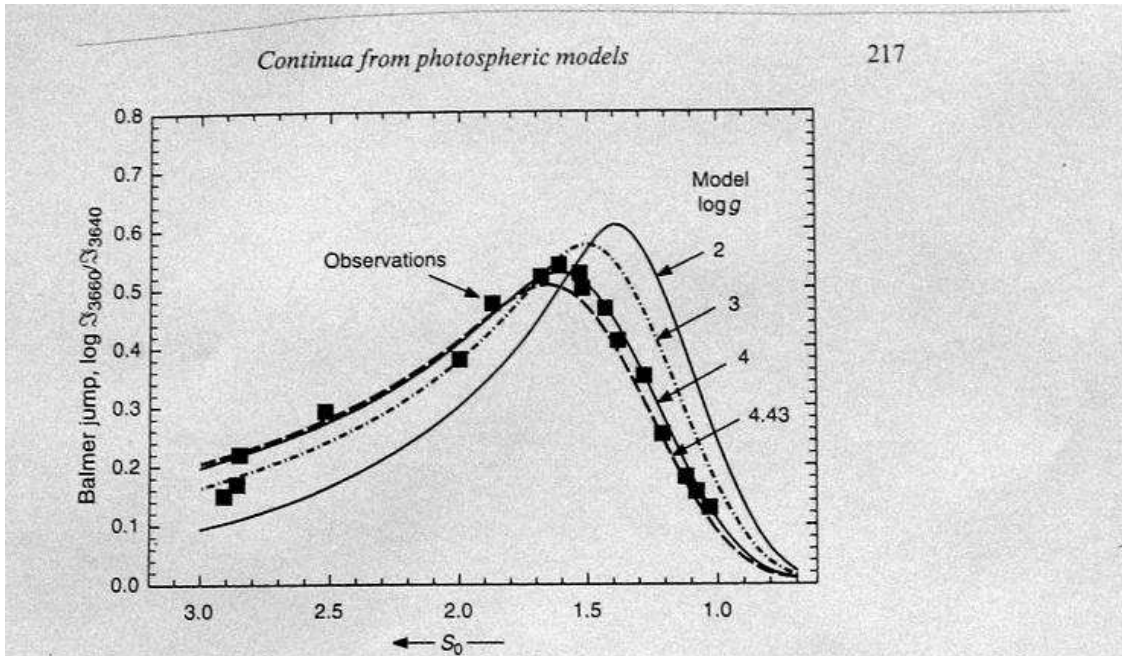
Fig. 10.9.   The Balmer jump depends on both temperature (S_0) and surface gravity (g). Solid lines are from scaled-solar models. The squares show the observations tabulated by Barbier (1958).   *from Gray, Stellar Photospheres 3rd ed*
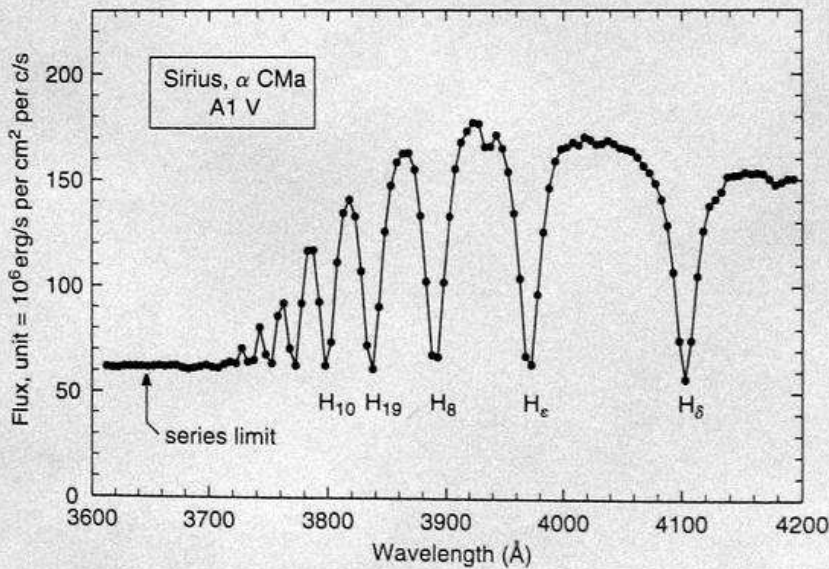
Fig. 10.10.   When the Balmer jump is strong, so are the Balmer lines. The lines obliterate the Paschen continuum near the series limit. At 5 Å resolution for the data, and with the relatively high surface gravity of Sirius, the lines disappear well above the series limit. Based on data from Panek (1977).

Fig. 18.— Upper panel: The Balmer jump as a function of T_{eff} and surface gravity. Lower panel: The Balmer lines in a star with $T_{eff} \sim 10,000$ K.

9. Microturbulence, Macroturbulence, Rotation

Microturbulence is small scale motions of the stellar gas, beyond the always present thermal motions, such that the local velocity is larger than the appropriate thermal velocity. The line absorption coefficient is affected in that the Doppler width parameter is then bigger than that corresponding to just the thermal velocity, $\sqrt{2kT/m}$. The non-thermal and thermal contributions add in quadrature to obtain the velocity width $\Delta\nu_D$ for the absorption line profile. Microturbulence affects the equivalent width of a spectral feature.

At $T = 6000$ K, the mean velocity of H atoms is 13 km/sec. For heavier atoms, $v \propto 1/\sqrt{m}$, and microturbulent velocities of order of 1 km/sec may substantially affect the "Doppler width" $\Delta\nu_D$.

Macroturbulence arises from large scale motions such as convection or rotation. (v_{rot} for the Sun is about 1.9 km/sec.) In this case the local value of the line absorption $\alpha(\nu)$ and of the predicted $I(\nu)$ is unaffected, but the velocity shifts this entire profile in frequency across the disk of the star depending on the local velocity with respect to the mean over the disk. The total flux at each frequency within the feature is then obtained by applying the appropriate frequency shift to the nominal line absorption profile (i.e. the local $I(\nu)$), which is itself constant, and integrating over the area of the disk. A more careful treatment would include limb darkening across the disk as well as the actual solid angle integral. The equivalent width of an absorption or emission feature is preserved, but the flux is redistributed in frequency around the line center.

In the ideal case, both micro and macroturbulence should be negligable, except for rotation. Neither has any substantive effect on the stellar continuum, only on discrete absorption or emission lines.

Solid body rotation about an axis perpendicular to the line of sight is fairly

straightforward to handle; see, for example, chapter 18 of Gray's book (3rd edition). One divides the visible disk of the star into strips parallel to the axis of rotation, so that each strip has a constant rotational velocity with a wavelength shift from the nominal line center λ_0 of $\Delta\lambda = \lambda_0 \, \omega \, x/c$, where x is the distance from the axis of rotation of the strip, $0 \leq x << R$, and ω is the angular velocity of the rotation at the surface of the star. The largest velocities and hence wavelength shifts are found at the limb of the star furthest from the rotation axis, one side approaching the observer, the other receding. But these strips have the smallest solid angle on the disk. The bulk of the material has a smaller velocity shift with respect to the mean for the star.

The integral of these strips across the disk of $I(\nu)$, where $I(\nu)$ is appropriately shifted in frequency within each strip, gives the total observed flux as a function of frequency across the line.

Rotationally broadened lines have a characteristic U shape and are easily picked out in high resolution spectra of stars by an experienced person if $v_{rot} \gtrsim 2v_D$, where the latter is the total Doppler velocity including any microturbulence. v_{rot} is straightforward to measure if the line profile is well resolved.

Only $v_{rot} sin(i)$ can be determined, where i is the inclination angle between the line of sight and the axis of rotation.